J. Fluid Mech. (1997), *vol.* 337, *pp.* 1–24

Effects of free-stream turbulence on surface pressure fluctuations in a separation bubble

By P. J. SAATHOFF[1] AND W. H. MELBOURNE[2]

[1] Centre for Building Studies, Concordia University, Montreal, Quebec H36 1M8 Canada

[2] Department of Mechanical Engineering, Monash University, Clayton, Victoria 3168, Australia

(Received 9 October 1990 and in revised form 17 October 1996)

Wind-tunnel experiments were conducted to investigate the cause of large pressure fluctuations near leading edges of sharp-edged bluff bodies. Measurements obtained with a blunt flat plate showed that very low pressures occur in a narrow region located approximately $0.25X_R$ from the leading edge, where X_R defines the distance from the leading edge to the mean reattachment location. This phenomenon occurs in the undisturbed flow as well as turbulent flow, although the magnitude of peak pressure fluctuations increases with both turbulence intensity, $\sigma_u/\bar{u}$, and turbulence scale, L_X.

Flow visualization experiments conducted with a high-speed cine-camera reveal the process that causes large pressure fluctuations in separation bubbles. This process is initiated when a perturbation in the approaching flow causes a roll-up of the separated shear layer, producing a strong vortex near the surface. Conditional sampling of pressure data was used to determine the spanwise length of the vortex. A significant increase in the spanwise correlation of pressure fluctuations occurs when the shear layer rolls up. Coherence measurements indicate that the spanwise length of vortices in the separation bubble is not directly related to longitudinal velocity fluctuations in the free-stream.

1. Introduction

The occurrence of large pressure fluctuations near leading edges of buildings is a major cause of damage in windstorms. Numerous wind-tunnel studies have shown that the magnitude of peak pressure fluctuations depends strongly on the level of free-stream turbulence (e.g. Melbourne 1979; Hunt 1982). However, the complexity of the flow around a building model makes it difficult to determine the relative significance of turbulence intensity and turbulence scale. As a result, the mechanism that causes peak pressure fluctuations to occur on streamwise surfaces has not been studied extensively.

In the present study, wind-tunnel experiments were conducted in uniform flow with a long two-dimensional rectangular prism, as shown in figure 1. This geometry was chosen because it greatly simplifies the study of separated/reattaching flows and has been used previously by a number of researchers (e.g. Kiya & Sasaki 1983*a*, *b*, 1985; Hillier & Cherry 1981; Nakamura & Ozono 1987). In this case, shear-layer reattachment is permanent and separation bubbles formed at the leading edges are unaffected by the flow over the opposite surface.

Hillier & Cherry (1981) investigated effects of free-stream turbulence on mean and fluctuating pressure distributions on a blunt flat plate. Results of that study showed that streamwise distributions of mean pressure in a separation bubble are strongly dependent on turbulence intensity, $\sigma_u/\bar{u}$. An increase in $\sigma_u/\bar{u}$ was shown to reduce the

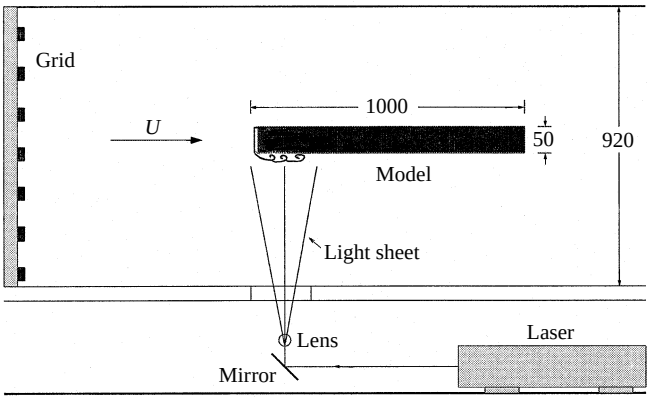

FIGURE 1. Experimental arrangement. (Dimensions in mm.)

mean reattachment length, X_R, causing a reduction in mean pressure at separation. The effect of turbulence scale, L_X, on mean pressure distributions and X_R was negligible for $0.36 < L_X/D < 1.95$, where D is the model thickness. On the other hand, an increase in L_X/D caused pressure fluctuations to increase in the separation bubble.

Cherry, Hillier & Latour (1984) made extensive measurements in a separation bubble formed on a blunt flat plate in smooth flow. Results of this study indicated that the unsteady flow in a separation bubble is dominated by three processes:

(i) a low-frequency flapping motion which occurs at a frequency, $n \approx 0.11\bar{u}/X_R$, where $\bar{u}$ is the mean free-stream velocity;
(ii) a pseudo-periodic shedding of vortices from the bubble with an average streamwise spacing of $0.7X_R$; and
(iii) an irregular shedding of large-scale vortices.

These conclusions generally agree with those of Kiya & Sasaki (1983*b*).

A number of studies have examined the influence of a periodic velocity perturbation on shear-layer behaviour. Results obtained by Parker & Welsh (1983) indicate that the inclusion of a sound field causes vortices to be shed from the separation bubble at the sound frequency, for rectangular prisms with chord/thickness ratios greater than 3:1. The presence of acoustic perturbations also causes a reduction in X_R and mean pressure near separation, similar to the effects of free-stream turbulence noted by Hillier & Cherry (1981).

Sigurdson & Roshko (1985) also studied the influence of an acoustic field on shear-layer behaviour. It was noted that the flow in a separation bubble is controlled by two instabilities:

(i) the Kelvin–Helmholtz shear-layer instability at an initial frequency, n_{KH}; and
(ii) a large-scale shedding of vorticity from the bubble over a range of frequencies centred at a dominant frequency, n_{shed}.

The shedding of large-scale vortices is amplified by a free-stream perturbation when the frequency of the perturbation matches n_{shed}.

A numerical simulation conducted by Hourigan *et al.* (1985) using the discrete vortex model found that large reductions in pressure occurred near the leading edge of a blunt flat plate when a fluctuating irrotational velocity field was included. The

simulation of the unsteady flow in the separation bubble and downstream of reattachment corresponded well with results of wind tunnel experiments in which a sound field was used to perturb the shear layers.

Results of these studies have provided considerable insight into characteristics of the unsteady flow in separation bubbles. The purpose of the present study is to examine how free-stream turbulence influences the behaviour of separated shear layers near the leading edge of a sharp-edged bluff body. In particular, the study is concerned with the relative influence of turbulence scale and turbulence intensity on the occurrence of very low pressures on streamwise surfaces. This topic has great significance for wind engineering applications.

2. Experimental methods

2.1. *The wind tunnel and model*

The model used in the study was a two-dimensional flat plate with a rectangular cross-section, as shown in figure 1. The plate had a thickness, D, of 50 mm and a chord/thickness ratio, L/D, of 20. The spanwise dimension, W, was 1.0 m, giving an aspect ratio, W/D, of 20. The model was mounted between end-plates and the angle of attack was adjusted so that streamwise mean pressure distributions on the top and bottom surfaces were equivalent to within $\pm 2\%$.

Experiments were carried out in a closed-circuit wind tunnel with a working section 4 m long, 1.24 m wide and 0.92 m high. The background turbulence intensity in the tunnel was 0.8 %. Free-stream turbulence was generated with three bi-planar wooden grids which had bar widths, b, of 70, 37, and 16 mm. The ratio of mesh size, m, to bar width was 4.0 for each grid. Turbulence parameters, shown in table 1, were measured using a Southampton constant temperature hot-wire anemometer.

Mean wind velocity at the model location was approximately 12.3 m s^{-1}, which was close to the maximum attainable when turbulence grids were used. Reynolds number based on model thickness ($Re = \rho\bar{u}D/\mu$) was approximately 4.0×10^4. Previous studies with this flow geometry have shown that measurements are independent of Reynolds number for $Re > 3.0 \times 10^4$ (Cherry *et al.* 1984; Gartshore & Djilali 1986).

Honeywell 163PC differential pressure transducers were used to measure surface pressure fluctuations on the model. The transducers were connected to pressure tappings with 60 mm lengths of PVC tubing with an internal diameter of 1.5 mm. Pressure tappings were made from 20 mm lengths of steel tubing with a bore of 1.08 mm. A restrictor was placed in the middle of the PVC tube to remove a resonant peak which occurred at a frequency of 480 Hz. The restrictor provided a flat frequency response $\pm 10\%$ up to 300 Hz and produced a phase lag which was approximately a linear function of frequency.

Mean, fluctuating and peak pressure coefficients are defined as $C_{\bar{p}} = (\bar{p} - p_0)/q$, $C\sigma_p = \sigma_p/q$, and $C_{\check{p}} = (\check{p} - p_0)/q$, respectively, where q is the dynamic pressure ($\frac{1}{2}\rho\bar{u}^2$), $\bar{p}$ is the mean surface pressure, σ_p is the standard deviation of surface pressure fluctuations, $\check{p}$ is the minimum surface pressure, p_0 is the free-stream static pressure at the model location, $\bar{u}$ is the mean wind velocity at the model location, and ρ is the density of air. Pressure and turbulence data were acquired and analysed using a Data Precision Data 6000 waveform analyser. The sampling frequency, n_S, was usually 1000 Hz. However, n_S was reduced to 500 Hz in the flow-visualization experiments. Values of $C_{\bar{p}}$, $C\sigma_p$ and $C_{\check{p}}$ were obtained by taking the ensemble average of 100 samples of 4.1 s duration.

Wind-tunnel blockage was 5.4 %. No corrections have been applied to the measurements owing to the lack of a satisfactory method for correcting pressure

	M (mm)	b (mm)	$\sigma_u/\bar{u}$ (%)	L_x (mm)
Grid A	280	70	8.0	105
			12.0	75
Grid B	148	37	8.1	45
			12.0	37
Grid C	64	16	8.2	20
			12.0	17
Undisturbed flow	—	—	0.8	—

TABLE 1. Turbulence characteristics for the different grids.

measurements on streamwise surfaces. However, results obtained by Saathoff & Melbourne (1987) indicate that a blockage ratio of 5% will increase $(1-C_{\bar{p}})$ by approximately 15% and cause $C\sigma_p$ and $(1-C_{\check{p}})$ to increase by 20%. However, effects of blockage are not expected to have a significant influence on conclusions regarding the effects of free-stream turbulence on streamwise pressure measurements.

Measurements of fluctuating surface pressures on wind-tunnel models are unavoidably affected by sources of noise in the wind tunnel. In the middle of the separation bubble, the error in $C\sigma_p$ owing to noise was estimated to be 2% in turbulent flow and 3% in the undisturbed flow. Thus, wind-tunnel acoustics did not have a significant effect on the pressure measurements. This is indicated by the very good comparison of fluctuating pressure data with the results of Cherry (1982) (see figure 5).

2.2. *The flow-visualization method*

The method of lighting the separation bubble is shown in figure 1. A cross-section of the bubble along the model centreline was illuminated by an intense sheet of light produced by passing the beam of a 5-watt argon laser through a cylindrical glass rod (6 mm diameter). The thickness of the sheet was approximately 2.5 mm. This technique has been used previously by Head & Bandyopadhyay (1981) to photograph flow structures in a turbulent boundary layer.

A high-speed Fastax 16 mm cine-camera (Model WF17) with Fuji ASA 500 colour film was used in the study. This camera was a combined framing/oscillographic camera which allowed simultaneous recording of the flow image and a pressure signal on the film. The recording of pressure fluctuations on the film was vital in matching the photographs with the corresponding pressure data. When the camera was activated, the film accelerated from rest to reach a maximum framing rate of over 600 frames per second (f.p.s.). However, the framing rate was virtually constant over short lengths of film. Timing marks recorded on the edge of the film at $\frac{1}{100}$ s intervals made it possible to measure the framing rate to within ± 1%. The average framing rate for sequences of photographs presented in this paper was approximately 500 f.p.s. This corresponds to an effective shutter speed of 0.67 m s.

A major disadvantage of using smoke to visualize the instantaneous flow in a separation bubble at moderately high Reynolds numbers ($Re > 10^4$) is that the smoke density must be large in order to observe a significant portion of the bubble. However, the use of thick smoke tends to obscure details of the flow in the bubble. It was thought that better results might be obtained if relatively large particles were used. In the present study, powder was emitted from a slot which was $0.06D$ (3 mm) from the leading edge. The slot was approximately 2 mm $\times$ 15 mm at the outlet where a wire grid was located to provide some impedance to the flow of powder. A steady flow was obtained by using an engraving tool to vibrate a metal plate in the slot. The frequency

of oscillation of the engraving tool was 100 Hz. The powder consisted primarily of four parts balsa dust and one part china clay. The mean diameter of china clay and balsa particles was of the order of 5 μm and 30 μm, respectively. The balsa dust was used so that particle streaks would be recorded on the film. The suitability of a particle for velocity measurements or flow visualization depends on the frequency range of interest. This study was concerned with relatively large-scale velocity fluctuations associated with the motion of separated shear layers. Pressure spectra measured near the leading edge of the model indicated that significant velocity fluctuations were confined to frequencies below 100 Hz.

Assuming the drag coefficient for a particle is given by Stokes Law:

$$C_D = 24/Re_p \tag{1}$$

where Re_p is the particle Reynolds number ($Re_p = \rho_f(u_f - u_p)\, d_p/\mu_f$), Merzkirch (1974) shows that the equation of motion of a particle is:

$$\frac{\mathrm{d}u_p}{\mathrm{d}t} = \frac{18\mu_f(u_f - u_p)}{\rho_p d_p^2} \tag{2}$$

where ρ_f is the fluid density, u_f is the fluid velocity, μ_f is the dynamic viscosity of the fluid, ρ_p is the density of the particle, d_p is the diameter of the particle, and u_p is the particle velocity.

Assuming u_f is a constant and $u_p = 0$ at time $t = 0$, the solution of (2) is:

$$u_p = u_f(1 - \mathrm{e}^{-t/\tau}) \tag{3}$$

where $\tau = \rho_p d_p^2/18\mu_f$ and is the time it takes for the particle to respond to a step-change in fluid velocity.

For a 30 μm balsa particle ($\rho_p \approx 160$ kg m^{-3}), the time lag is approximately 0.14 ms. Assuming particles will follow velocity fluctuations up to a limiting frequency, $n_L \approx 1/8\tau$, a typical balsa particle will follow velocity fluctuations up to a frequency of approximately 250 Hz. From equation (2), the response time of a particle is proportional to d_p^2. Therefore, despite the relatively high density of china clay ($\rho_p \approx 2700$ kg m^{-3}), these particles have a significantly higher limiting frequency than the balsa particles. Assuming a mean particle size of 5 μm, the value of n_L for the china clay particles is of the order of 600 Hz. Thus, the balsa dust/china clay mixture is acceptable for this flow-visualization study. The particles will follow velocity fluctuations at frequencies significantly greater than those associated with large-scale motions of the separated shear layer.

Several studies (Parker & Welsh 1983; Sigurdson and Roshko 1985) have shown that acoustic sources may significantly affect the flow over sharp-edged bluff bodies in a wind tunnel. However, any acoustic effect produced by the vibrating plate (used to release the powder) is believed to be small. Pressure spectra measured near separation in turbulent flow ($\sigma_u/\bar{u} \approx 8.0\,\%$, $L_X/D \approx 2.1$) with and without the vibrating plate are virtually identical, as shown in figure 2. Likewise, measurements of $C_{\bar{p}}$ and $C_{\check{p}}$ were unaffected by the vibrating plate. Thus, it can be assumed that the vibrating plate did not influence the flow around the model.

Melbourne (1979) has shown that placing a slot in the eaves of a low-rise building model will reduce pressure fluctuations near the leading edge. In the present study, the slot attenuated the negative peak pressures to some extent, although the effect diminished with increasing distance from the leading edge. The slot reduced C_{σ_p} and $C_{\check{p}}$ at the closest tapping by less than 5%.

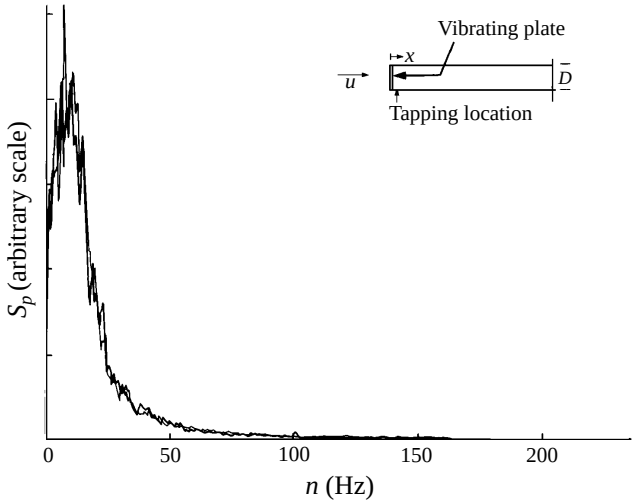

FIGURE 2. Effect of vibrating plate on pressure spectrum measured near separation ($\sigma_u/\bar{u} = 0.080$, $L_x/D = 2.1$): ——, with vibrating plate; ——, without vibrating plate.

3. Results

3.1. *Pressure distributions*

Streamwise profiles of the standard deviation pressure coefficient, C_{σ_p}, are shown in figure 3. An increase in $\sigma_u/\bar{u}$ causes pressure fluctuations to increase and the location of maximum C_{σ_p} to move closer to the leading edge. As shown by Hillier & Cherry (1981) and Kiya & Sasaki (1983*a*), the peak in the C_{σ_p} profile is located slightly upstream of X_R. A number of previous studies have shown that an increase in $\sigma_u/\bar{u}$ causes the mean reattachment length (X_R) to decrease (e.g. Hillier & Cherry 1981; Kiya & Sasaki 1983*a*). Data obtained by Saathoff (1989) for the present flow geometry are presented in figure 4. Results of Cherry (1982) are also shown and compare well with values of X_R from the present study, despite the differences in blockage ratio. (Blockage ratios were 3.8 % and 5.4 % for Cherry's study and the present work, respectively.) An increase in L_X/D causes C_{σ_p} to increase and this effect becomes greater as $\sigma_u/\bar{u}$ increases. Results obtained with short axi-symmetric cylinders by Saathoff & Melbourne (1987) have shown that C_{σ_p} correlates well with the empirical parameter, $\eta = (\sigma_u/\bar{u})\ (L_X/D)^{0.15}$, for $L_X/D < 2.1$. For the present geometry, values of C_{σ_p} measured near separation also correlate well with η. Data of Saathoff (1989) and Cherry (1982) are plotted in figure 5 and show good agreement. Cumulative distributions of $C_{\check{p}}$ measured near separation in large-scale turbulence ($\sigma_u/\bar{u} \approx 0.12$, $L_X/D \approx 1.5$) and small-scale turbulence ($\sigma_u/\bar{u} \approx 0.12$, $L_X/D \approx 0.35$) are shown in figure 6. As suggested by Holmes (1984), the data are plotted as a function of the reduced variate,

$$\bar{x} = -\ln[-\ln\{(i-0.44)/(N+0.12)\}], \tag{4}$$

where N is the number of samples ($N = 100$) and i is the rank order ($i = 1$ for the smallest $-C_{\check{p}}$ measured and $i = 100$ for the largest $-C_{\check{p}}$). This plotting method, developed by Gringorten (1963), approximates an unbiased plotting formula for the Type I extreme value distribution. The peak pressure coefficient can be expressed as a function of $\tilde{x}$:

$$C_{\check{p}} = M + (1/a)\,\tilde{x}, \tag{5}$$

where M is the mode and $(1/a)$ is the dispersion. An increase in L_X/D by a factor of

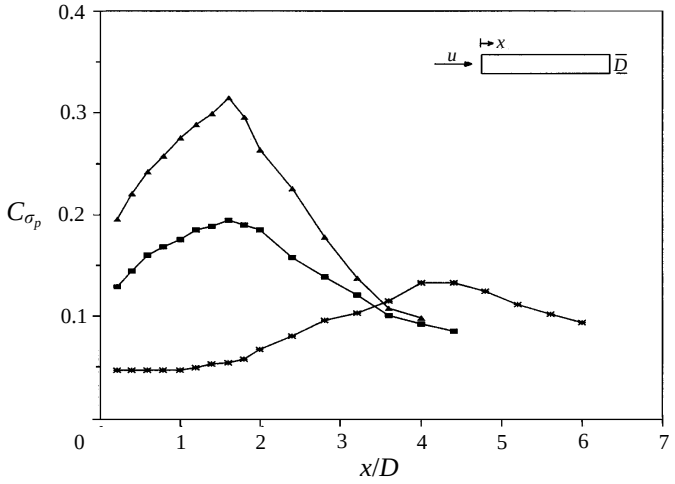

FIGURE 3. Influence of turbulence intensity and scale on streamwise distribution of fluctuating pressure coefficient (▲, $\sigma_u/\bar{u} = 0.080$, $L_x/D = 2.1$; ■, $\sigma_u/\bar{u} = 0.082$; $L_x/D = 0.4$; *, $\sigma_u/\bar{u} = 0.008$).

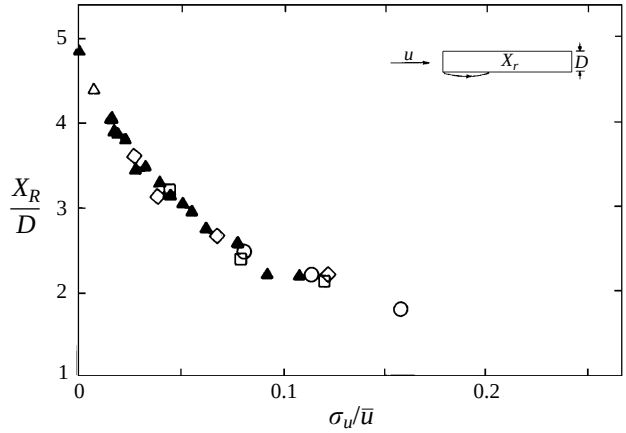

FIGURE 4. Mean reattachment length as a function of turbulence intensity.
○, Grid A; □, Grid B; ◇, Grid C; △, undisturbed flow; ▲, Cherry (1982).

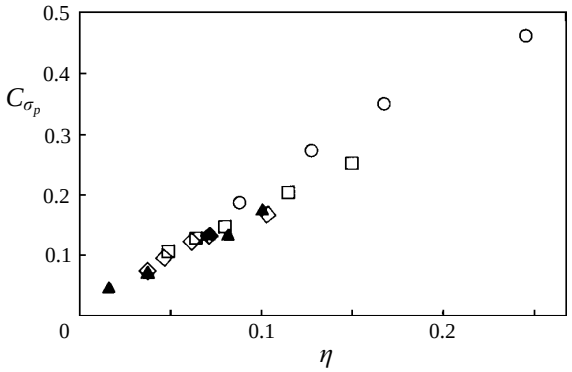

FIGURE 5. Fluctuating pressure coefficient near separation as a function of the turbulence parameter, $\eta = \sigma_u/\bar{u}(L_x/D)^{0.15}$. ○, Grid A; □, Grid B; ◇, Grid C; ▲, Cherry (1982).

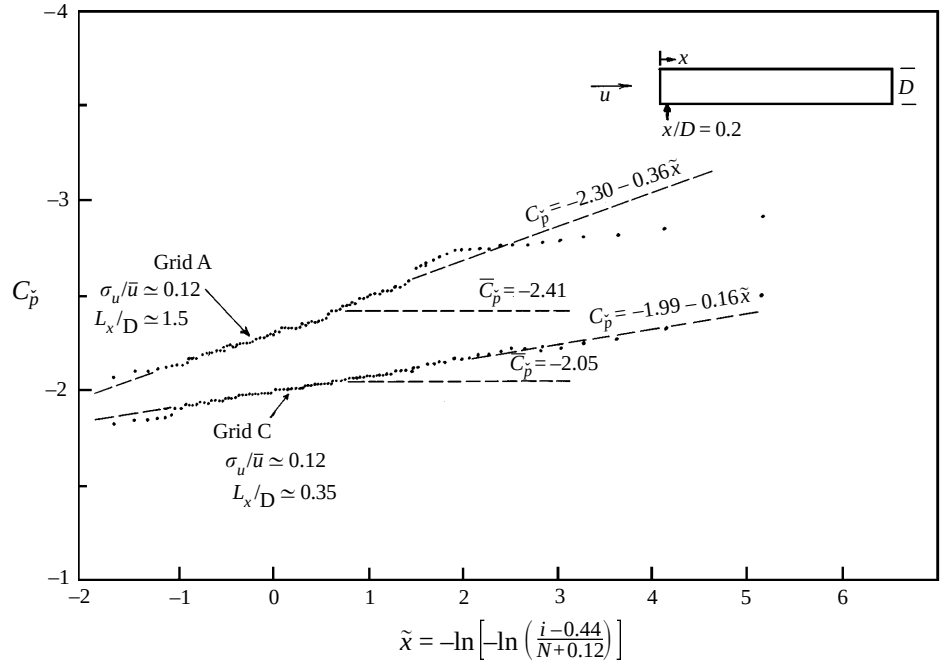

FIGURE 6. Cumulative distributions of peak pressure coefficient measured near separation in large-scale and small-scale turbulence.

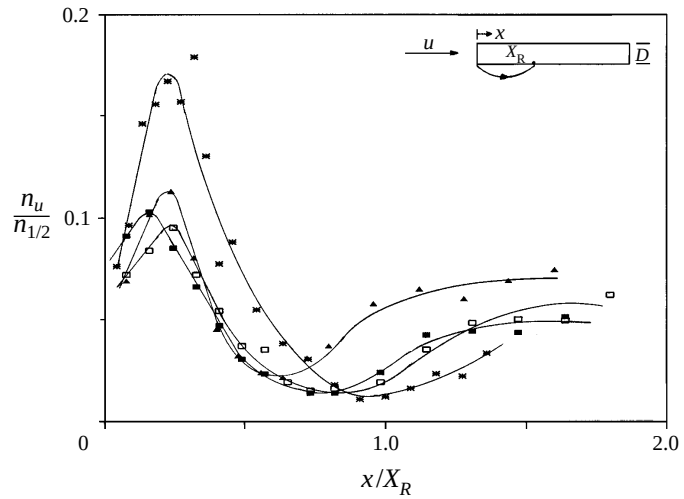

FIGURE 7. Distributions of normalized upcrossing frequency of peak pressure fluctuations. ▲, $\sigma_u/\bar{u} = 0.080$, $L_x/D = 2.1$; □, $\sigma_u/\bar{u} = 0.81$, $L_x/D = 0.9$; ■, $\sigma_u/\bar{u} = 0.082$, $L_x/D = 0.4$; *, $\sigma_u/\bar{u} = 0.008$.

four increases $-(1/a)$ from 0.16 to 0.36. The value of M is approximately 20% larger in the large-scale flow.

This study is concerned mainly with the mechanism which produces low-pressure peaks in the separation bubble. Kiya & Sasaki (1983*a*) show that distributions of pressure fluctuations are negatively skewed in a relatively narrow region where $|C_{\check{p}}|$ reaches a maximum. Their results indicate that this phenomenon is independent of

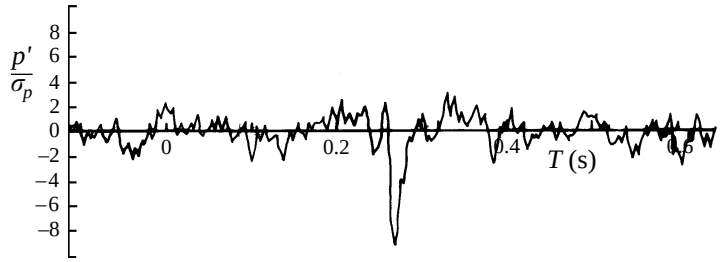

FIGURE 8. Typical large pressure drop measured in undisturbed flow in region of maximum $-C_{\check{p}}$ (tapping located at $x/X_R = 0.32$).

$\sigma_u/\bar{u}$ for models with a large chord/thickness ratio. An upcrossing analysis was conducted to determine where large pressure drops occur most often in the separation bubble. A threshold level was chosen such that $\check{p} < \bar{p} - 3\sigma_p$ and the upcrossing frequency, n_u was determined at each streamwise location. In figure 7, n_u is plotted as a function of distance from the leading edge, x, for the undisturbed and turbulent flows. Upcrossing frequency has been normalized with the half-power frequency, $n_{\frac{1}{2}}$, of the pressure spectrum measured at each tapping. The half-power frequency is the frequency which divides the power spectrum into two equal areas. Similarity between separation bubbles formed in the undisturbed flow and turbulent flow is evident when data are plotted as a function of x/X_R. The region where low-pressure peaks occur most often, as denoted by the peak in upcrossing frequency, is centred at $x \approx 0.25X_R$. Pressure fluctuations in this region tend to be highly intermittent as shown in figure 8.

3.2. *Flow visualization results*

3.2.1. *Undisturbed flow*

Numerous experiments were conducted in the undisturbed flow and turbulent flows to observe the behaviour of separated shear layers near the leading edge of the model. Figure 9 shows a series of photographs obtained in the undisturbed flow when a large pressure drop was recorded at $x/D = 1.52$ ($x/X_R \approx 0.35$). Included in figure 9 are pressure data associated with each frame, given in terms of p'/σ_p. The data were measured at tappings A, B and C, located $1.12D$, $1.52D$ and $1.92D$ from the leading edge, respectively. Wool tufts can be seen on the surface of the model at $x = 1.0D$ and $x = 2.0D$. The framing rate for this sequence was approximately 600 f.p.s. (The line that passes vertically through most of the frames is an oscilloscope trace of the pressure signal at tapping B. The oscilloscope trace lags approximately six frames behind the photograph associated with it.) It should be remembered that, in terms of C_{σ_p} and $C_{\check{p}}$, the pressure fluctuations shown in figure 9 are small compared to those obtained in turbulent flow. Values of C_{σ_p} and $C_{\check{p}}$ at tapping B were only 0.055 and -1.1, respectively.

The process that causes the large pressure fluctuation at tapping B, shown schematically in figure 10, is initiated in F2 when the shear layer rolls up to form a vortex near the leading edge. The vortex is shown clearly in F5, located at $x \approx 1.03D$. Flow reattachment is evident at $x \approx 1.5D$ and is accompanied by a positive pressure peak at tapping B. A relatively small pressure drop is measured at tapping A (F8), followed by a much larger pressure drop at tapping B (F9–F13). The negative peak at tapping B is larger than at tapping A mainly because the vortex is closer to the surface as it passes over tapping B. The very large negative peak at tapping B may also be a result of the lack of movement of the vortex. It appears to be stationary over tapping

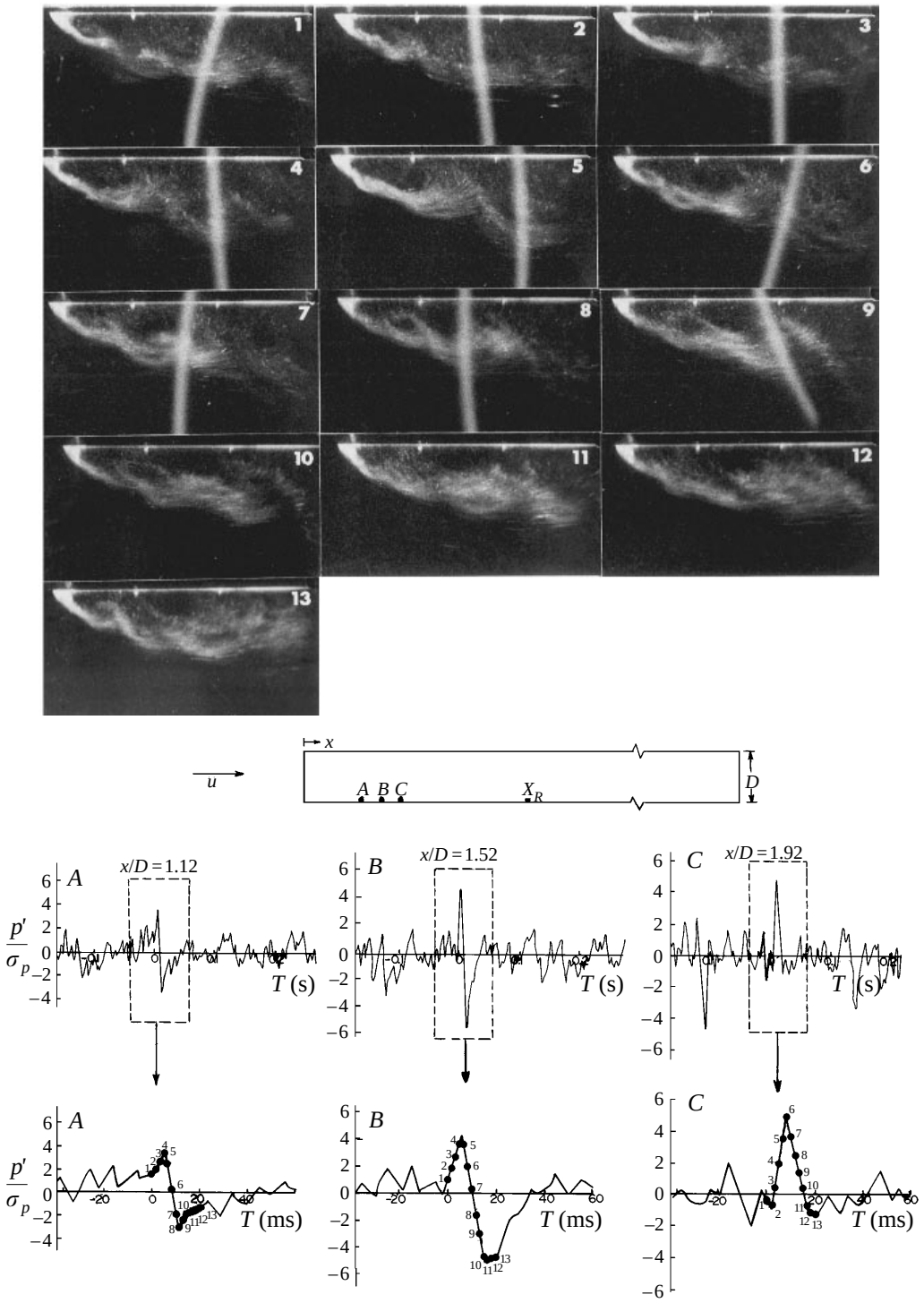

FIGURE 9. A sequence of photographs taken when a large pressure fluctuation occurred near the leading edge in undisturbed flow (lower pressure records are expanded versions of upper records; the time of occurrence of each frame is indicated on the lower records).

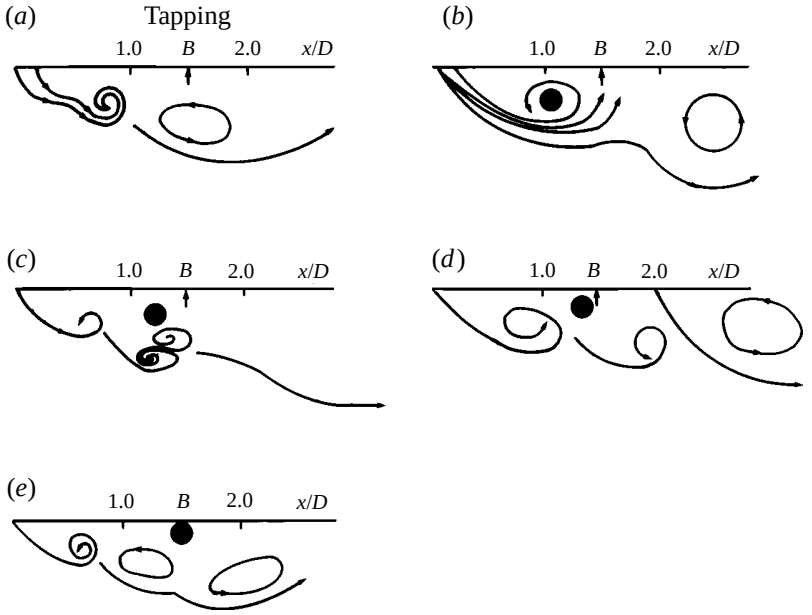

FIGURE 10. The formation and convection of the vortex that caused the large pressure fluctuation shown in figure 9. ●, location of the vortex, (*a*) Frame 2; (*b*) Frame 5; (*c*) Frame 7; (*d*) Frame 9; (*e*) Frame 13.

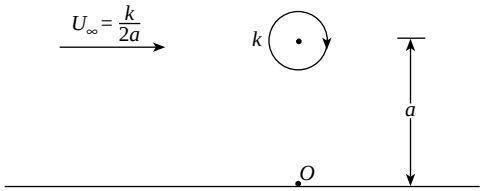

FIGURE 11. A stationary vortex filament above a plane surface.

B in F10–F13, and the pressure fluctuations measured at tapping *C* show that the vortex does not convect downstream. In F13, the pressure at tapping *C* reaches a small negative peak, but the vortex is still located over tapping *B*, as indicated by the magnitude of the pressure drop at that location.

Using potential flow theory it can be shown (Milne-Thomson 1960, p. 360) that a rectilinear vortex with strength, $-k$, located a distance, a, from a plane surface will move to the left at a speed $2k/a$, owing to the presence of the image vortex. If a free-stream velocity of $U_\infty = k/2a$ to the right is superimposed, the vortex will be stationary. This is shown schematically in figure 11. The pressure produced by the vortex at point O on the surface is given by:

$$P = P_\infty - \rho_f k^2/a^2, \tag{6}$$

where P_∞ is the upstream pressure. Equation (6) indicates that the pressure drop produced by a vortex is inversely proportional to a^2. Thus, a vortex that passes close to the surface will produce a much larger pressure drop than the same vortex convecting further out in the shear layer.

The pressure rise that occurs at tapping *B* after F13 may not be a result of the convection of the vortex downstream. Doligalski & Walker (1984) have shown that a stationary vortex near a surface causes a lift-up of the boundary layer, producing a

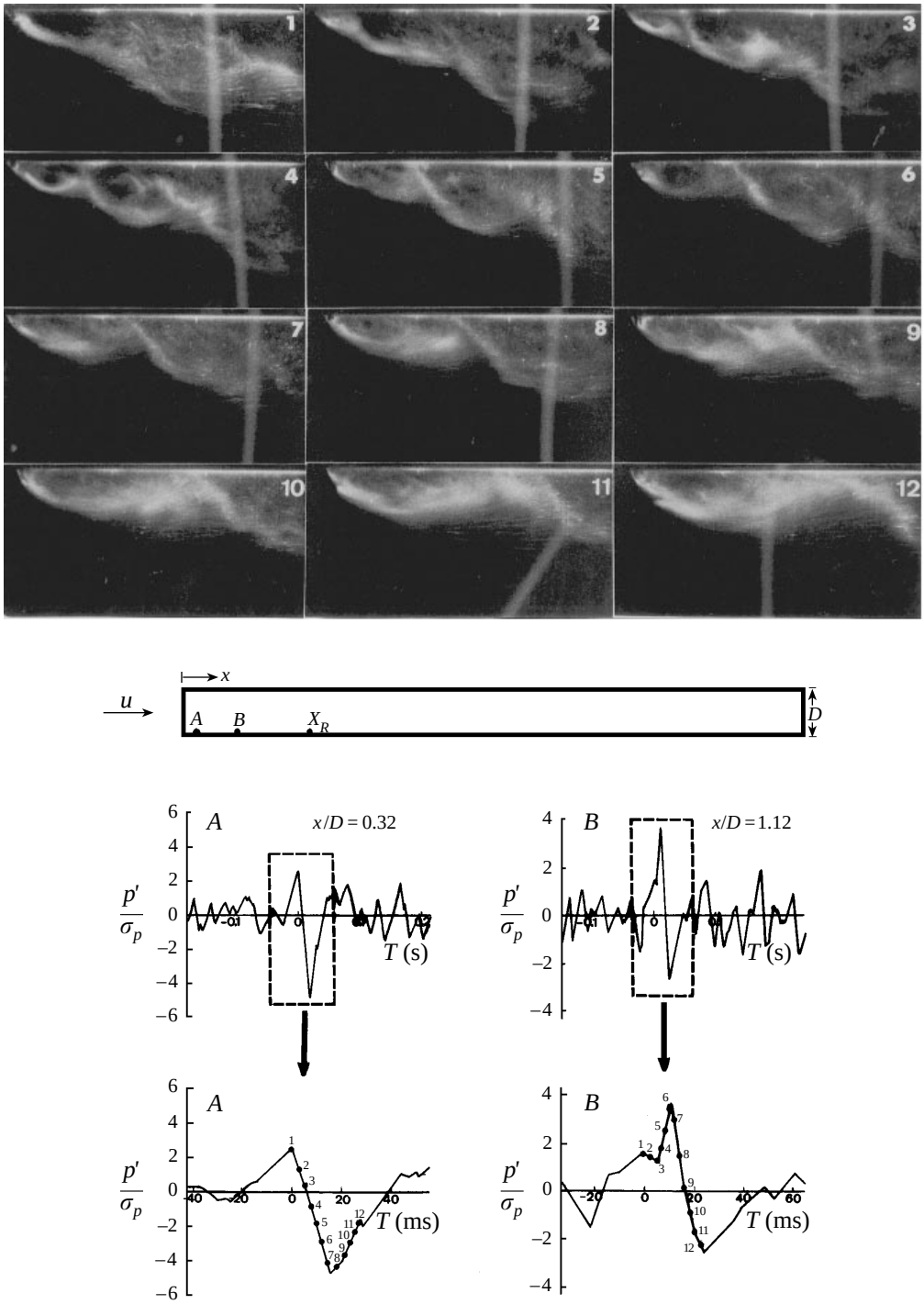

FIGURE 12. A sequence of photographs taken when a large negative pressure fluctuation occurred near the leading edge in large-scale turbulence. $\sigma_u/\bar{u} = 0.080$; $L_x/D = 2.1$.

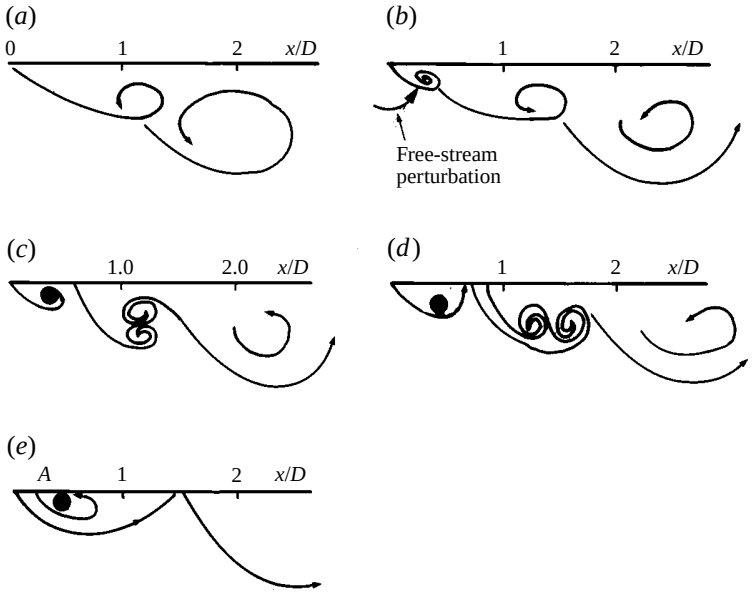

FIGURE 13. The formation and convection of the vortex that caused the large pressure fluctuation shown in figure 12. (*a*) Frame 1; (*b*) Frame 2; (*c*) Frame 3; (*d*) Frame 4; (*e*) Frame 8, minimum pressure at tapping *A*.

secondary vortex rotating in the opposite direction. The increase in pressure at tapping *B* may be associated with the entrainment of vorticity of opposite sign into the parent vortex.

Gartshore (private communication, 1988) notes that streamwise vorticity will be associated with the roll-up of the shear layer and the process which produces low-pressure peaks in the separation bubble. The growth of streamwise vortices in a plane, free shear layer has been investigated by Lasheras, Cho & Maxworthy (1986) in a flow-visualization study. Their results show that streamwise vortices are superimposed on the spanwise vortices and are produced by the unstable response of the shear layer to three-dimensional perturbations in the free stream.

3.2.2. *Turbulent flow*

A series of photographs obtained in large-scale turbulence (Grid A: $\sigma_u/\bar{u} \approx 8.0\,\%$, $L_X/D \approx 2.1$) when the shear layer rolled up close to the leading edge as shown in figure 12. Also shown are pressure records measured at tapping *A* and tapping *B* at $x/D = 0.32$ and $x/D = 1.12$, respectively. The framing rate for this series was approximately 450 f.p.s.

The process that produced the large reductions in pressure at tapping *A* and tapping B is shown schematically in figure 13. A comparison of F1 and F2 indicates that some perturbation (presumably in the free-stream flow) has forced the shear layer to move close to the surface. A new separation bubble has formed in F3–F4 well upstream of the mean reattachment location ($X_R \approx 2.45D$). The high curvature of the flow near the leading edge in F4 indicates the presence of a strong vortex. This vortex grows in size and gains strength as it entrains vorticity. The increase in strength of the vortex, as well as its proximity to the surface, produces a large pressure drop at tapping *A* ($C_{\check{p}} \approx -2.1$) in F7–F8, followed by a slightly smaller peak ($C_{\check{p}} \approx -1.8$) at tapping *B* in F12. Note that pressure fluctuations in this flow are significantly larger in magnitude than those

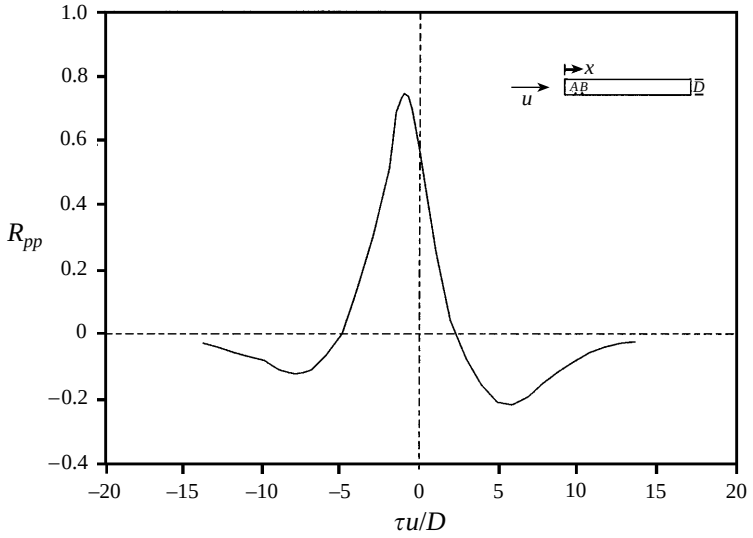

FIGURE 14. Cross-correlation of fluctuating pressure measured at $x/D = 0.6$ and $x/D = 1.0$ in turbulent flow. $\sigma_u/\bar{u} = 0.080$; $L_x/D = 2.1$.

recorded in the undisturbed flow. From figure 3, values of C_{σ_p} at tapping A and tapping B are 0.22 and 0.285, respectively. The cause of the large pressure rise at tapping B is illustrated in F4–F7. As the new bubble forms, a large vortex is shed and convects downstream. The maximum pressure at tapping B occurs when the tail of the shed vortex passes over it in F6.

Figure 14 shows the correlation coefficient, R_{pp}, as a function of time lag for pressure fluctuations measured at $x/D = 0.6$ and $x/D = 1.0$. The time lag between $T = 0$ and the peak in R_{pp} indicates the average convection speed of the vortices, u_c. In this case, $u_c \approx 0.43\bar{u}$ which corresponds well with the value of u_c of $0.4\bar{u}$ obtained by Cherry (1982) in smooth and turbulent flows.

A series of photographs and corresponding pressure signals obtained in small-scale turbulence ($\sigma_u/\bar{u} \approx 8.2\%$, $L_X/D \approx 0.4$) are shown in figure 15. Pressure fluctuations were measured at tappings A, B and C, which were located $0.32D$, $0.72D$ and $1.12D$ from the leading edge, respectively. The framing rate was approximately 490 f.p.s. The photographs were taken when a relatively large pressure reduction ($C_{\check{p}} \approx -1.6$) occurred at tapping B. The value of C_{σ_p} at tapping B was approximately 0.17. Pressure fluctuations in this flow are smaller in magnitude than those obtained in the large-scale flow with the same $\sigma_u/\bar{u}$, as indicated in figure 3. Note that the pressure data shown in figure 15 are not well correlated in the streamwise direction, compared to data obtained in the large-scale flow, shown in figure 12. In F6 of figure 15, the flow has apparently reattached close to the leading edge. The pressure decreases at tapping B as vorticity in the new bubble increases. However, in F10–F11 the shear layer rolls up to form a second new bubble near separation. The vortex that produced the large pressure drop is shed downstream in F11–F12, causing the pressure to rise at tapping B.

Comparison of figure 15 with figure 12 illustrates how a reduction in turbulence scale reduces the magnitude of $C_{\check{p}}$. In the small-scale flow, the shear layer is subjected to relatively high-frequency perturbations. As a result, vortices formed near the leading edge are shed downstream before they attain significant strength. The higher shedding frequency in the small-scale flow is indicated by an increase in characteristic frequency of negative peaks, $\check{n}$. Based on samples of 300 negative peaks exceeding σ_p, $\check{n} \approx 45$ Hz

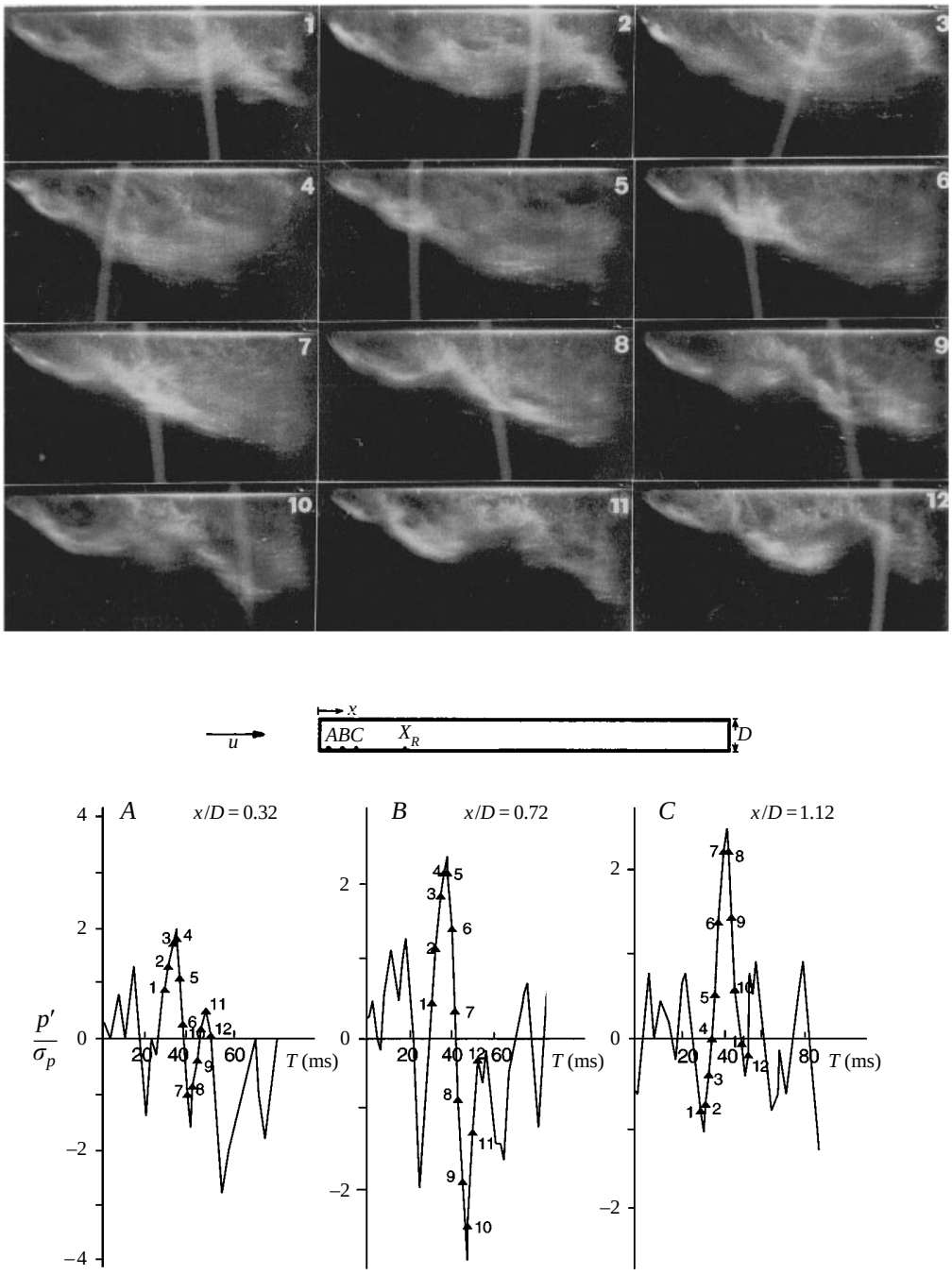

FIGURE 15. A sequence of photographs taken when a large negative pressure fluctuation occurred near the leading edge in small-scale turbulence. $\sigma_u/\bar{u} = 0.082$; $L_x/D = 0.4$.

in the small-scale flow and $\check{n} \approx 30$ Hz in the large-scale flow. Thus, an increase in turbulence scale by a factor of five has caused the duration of a typical peak, $\check{\tau}$, to increase by approximately 50 %. In other words, the period of vorticity entrainment for a vortex in the large-scale flow is, on average, 1.5 times that for a vortex in the small-

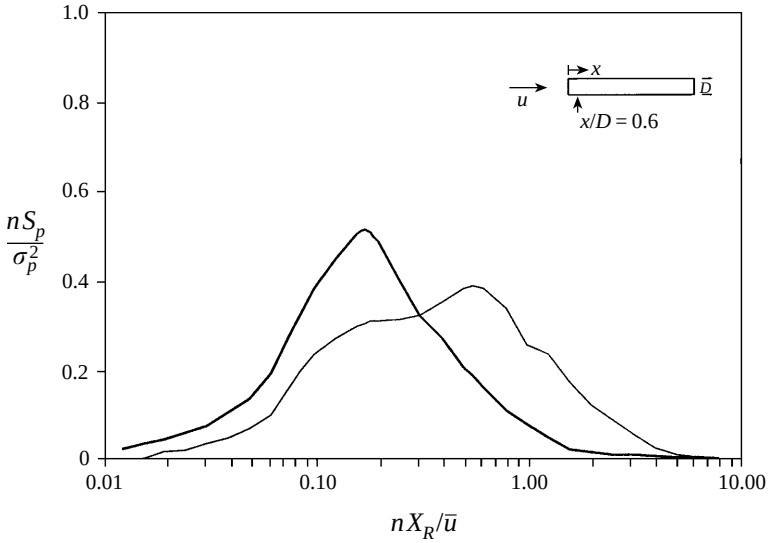

FIGURE 16. Pressure spectra measured in large-scale and small-scale turbulence ——, $\sigma_u/\bar{u} = 0.080$, $L_x/D = 2.1$; ——, $\sigma_u/\bar{u} = 0.082$, $L_x/D = 0.4$.

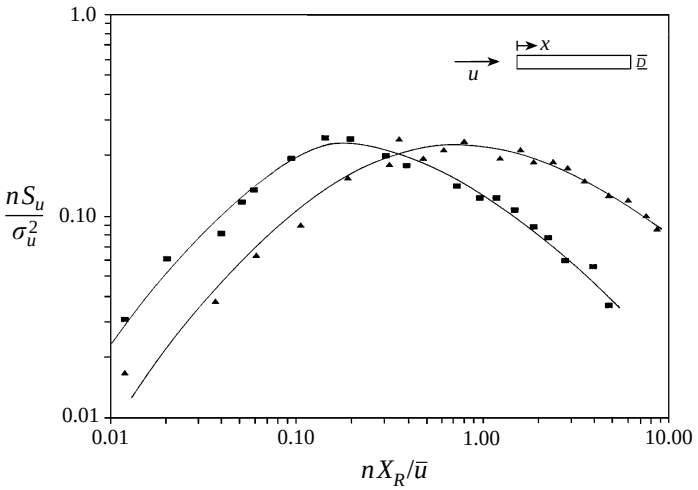

FIGURE 17. Longitudinal velocity spectra measured in large-scale and small-scale turbulence. ▲, $\sigma_u\bar{u} = 0080$, $L_x/D = 2.1$; ■, $\sigma_u/\bar{u} = 0.082$, $L_x/D = 0.4$.

scale flow. Sigurdson & Roshko (1985) and Parker & Welsh (1983) have shown that a fluctuating sound field affects separated shear layers in much the same way as free-stream turbulence. Their flow-visualization experiments indicate that the shedding frequency of the bubble can be controlled by the sound frequency.

Pressure spectra measured at $x/D = 0.6$ in large-scale and small-scale turbulence are shown in figure 16. Turbulence spectra for these two flows are presented in figure 17. The pressure spectrum obtained in the small-scale flow has a broad maximum at $nX_R/\bar{u} \approx 0.16$ and another peak at $nX_R/\bar{u} \approx 0.55$ ($X_R \approx 2.45D$ for both flows). The high-frequency peak coincides roughly with the peak in the turbulence spectrum. The low-frequency hump is probably associated with the low-frequency unsteadiness of the separation bubble, which has been shown to be a common feature of separated/

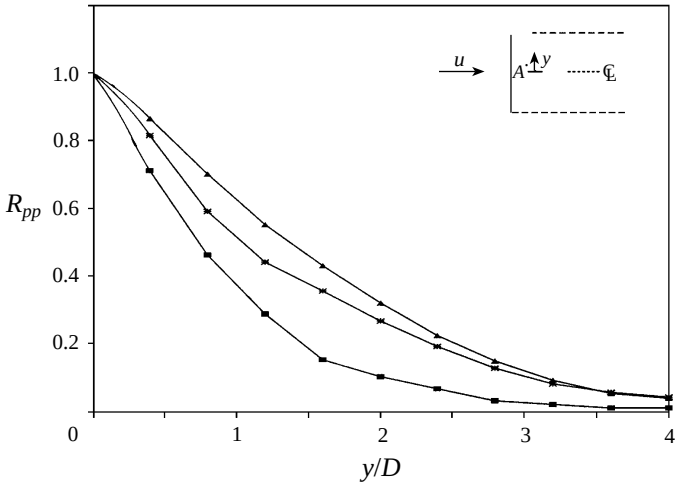

FIGURE 18. Cross-correlation of fluctuating pressure as a function of lateral displacement. ▲, $\sigma_u/\bar{u} = 0.080$, $L_x/D = 2.1$; ■, $\sigma_u/\bar{u} = 0.082$, $L_x/D = 0.4$; *, $\sigma_u/\bar{u} = 0.008$.

reattaching flows. Results obtained by Cherry *et al*. (1984) and Kiya & Sasaki (1983*b*) indicate that this unsteadiness occurs at $nX_R/\bar{u} \approx 0.12$, for a blunt flat plate in smooth flow.

On the other hand, the pressure spectrum obtained in the large-scale flow has one dominant peak located at $nX_R/\bar{u} \approx 0.16$. This peak coincides with the peak in the turbulence spectrum and is also close to the characteristic frequency of the low-frequency unsteadiness of the separation bubble. This influence of turbulence scale on pressure spectra measured in a separation bubble has been discussed previously by Hillier & Dulai (1985).

The increase in magnitude of pressure fluctuations as L_X/D increases is possibly related to the interaction of free-stream perturbations with the low-frequency unsteadiness of the separation bubble. An increase in turbulent energy at frequencies near that of the low-frequency unsteadiness may enhance the roll-up of the shear layer.

Future experiments should be conducted in very large-scale turbulent flows ($L_X/D > 5$) to determine if pressure fluctuations continue to increase with increasing turbulence scale. Presumably, if the occurrence of shear layer roll-up is dependent on the phase of the low-frequency motion of the bubble, free-stream perturbations at frequencies near $0.15\bar{u}/X_R$ should have the most influence on the shear layer.

3.3. *Lateral pressure cross-correlations*

An indication of the spanwise extent of vortices in the separation bubble is given by the cross-correlation coefficient, R_{pp}, defined as:

$$R_{pp} = \frac{\overline{p_1' p_2'}}{\sigma_{p1}\sigma_{p2}}, \tag{7}$$

where p_1' is the fluctuating pressure measured at tapping 1, p_2' is the fluctuating pressure measured at tapping 2, σ_{p1} and σ_{p2} are the standard deviations of p_1' and p_2', and the overbar indicates a time-averaged quantity.

Figure 18 shows R_{pp} as a function of lateral displacement, y/D, in the region of maximum negative peak pressures. A progressive decrease in R_{pp} with turbulence scale is evident. Correlation lengths, $L_y = \int_0^\infty R_{pp}\,\mathrm{d}y$, for the undisturbed flow and three

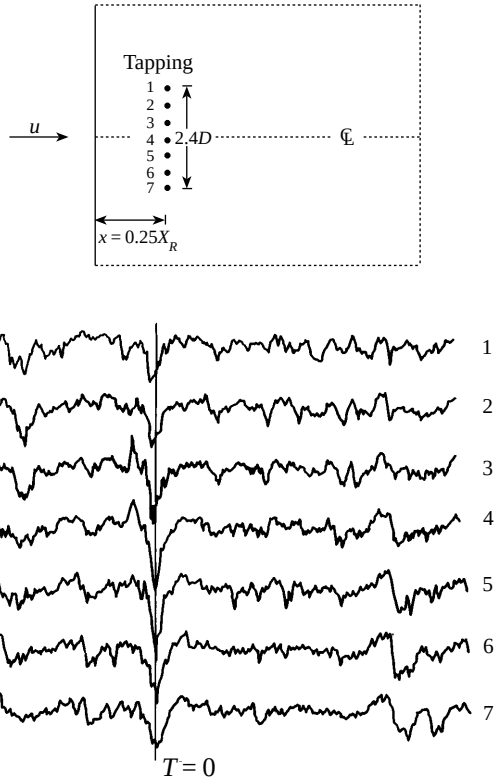

FIGURE 19. Simultaneous pressure records obtained at seven tappings near the leading edge when a large presure drop occurred at tapping 4 at time $T = 0$ s. $\sigma_u/\bar{u} = 0.080$, $L_x/D = 2.1$.

$\sigma_u/\bar{u}$	L_x/D	L_y/D	L_y/X_R	L_y^*/D
8.0(%)	2.1	1.6	0.65	2.4
8.1(%)	0.9	1.3	0.50	—
8.2(%)	0.4	1.0	0.40	1.4
0.8(%)	—	1.5	0.35	2.2

TABLE 2. Correlation lengths of spanwise pressure fluctuations

turbulent flows are presented in table 2. Values of L_y for the undisturbed flow and the small-scale turbulent flow are approximately $0.4X_R$, and even in the large-scale flow, L_y is only $0.65X_R$. Thus, on average, the flow near the leading edge is highly three-dimensional.

For wind engineering applications, it is important to determine whether the flow is significantly more two-dimensional when very large pressure fluctuations occur. The spanwise length of vortices which produce very large pressure fluctuations is indicated in figures 19–21 for the large-scale, small-scale and undisturbed flows, respectively. Pressure traces at seven tappings, located approximately $0.25X_R$ from the leading edge, were recorded simultaneously when an extremely large negative peak ($p' < \bar{p} - 4\sigma_p$) was measured at the centre tapping. The lateral spacing between tappings was $0.4D$, giving a total spanwise separation of $2.4D$.

In the large-scale turbulent flow (figure 19), large pressure drops were recorded at the

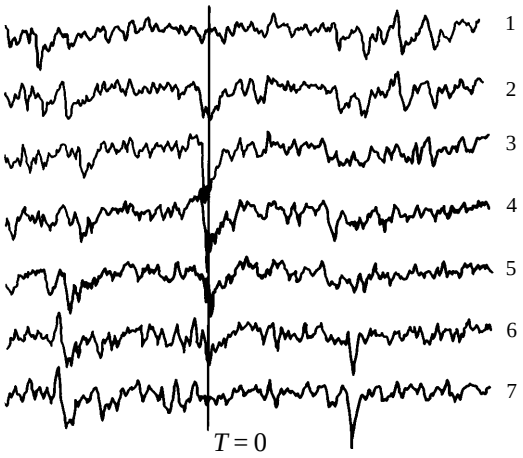

FIGURE 20. Simultaneous pressure records obtained at seven tappings near the leading edge when a large pressure drop occurred at tapping 4 at time $T = 0$ s. $\sigma_u/\bar{u} = 0.082$, $L_x/D = 0.4$.

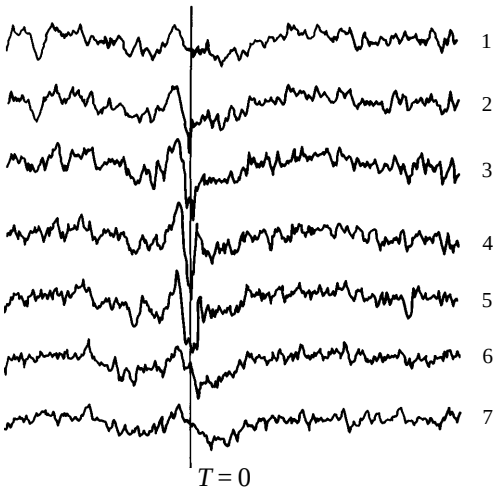

FIGURE 21. Simultaneous pressure records obtained at seven tappings near the leading edge when a large pressure drop occurred at tapping 4 at time $T = 0$ s. (Undisturbed flow: $\sigma_u/\bar{u} = 0.008$.)

other six tappings when a large negative peak occurred at the centre tapping. Therefore, the spanwise length of the vortex was probably at least $3.0D$ or approximately $1.2X_R$. (Note the small phase difference in the signals which indicates a slight streamwise inclination of the vortex.) On the other hand, figure 20 shows that small-scale turbulence causes the flow to be more three-dimensional. In this case, the vortex that produced the large pressure drop at the centre tapping had a spanwise length of only $2.0D$ or $0.8X_R$. Likewise, in the undisturbed flow, peak pressure fluctuations are not well correlated in the spanwise direction. In figure 21, a large negative peak at the centre tapping coincides with pressure drops at only three of the other tappings, although the initial pressure rise preceding the negative peak occurs at all tappings.

The degree of instantaneous correlation between two fluctuating signals, p_1' and p_2', can be determined by examining the time trace of their product, $p_1' p_2'$. Instances of high

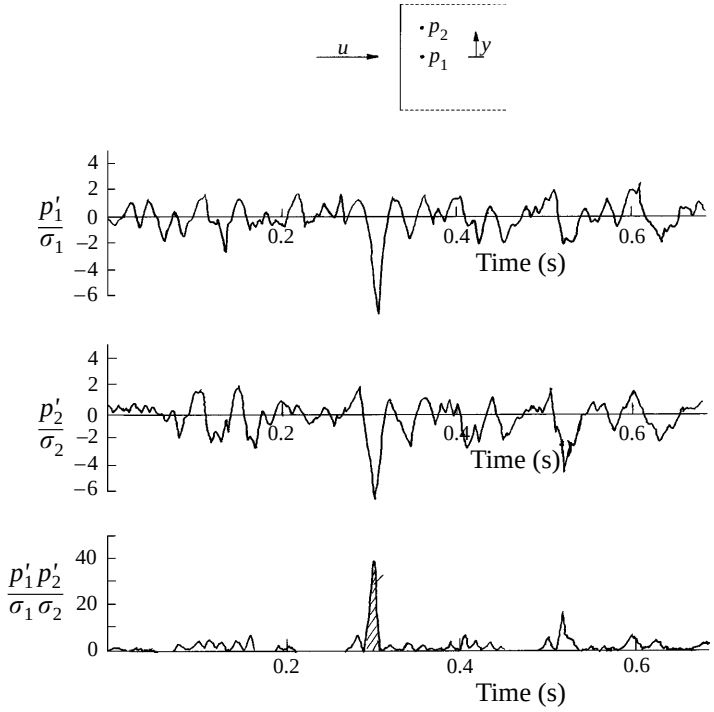

FIGURE 22. Two pressure signals obtained simultaneously showing occasional high correlation.

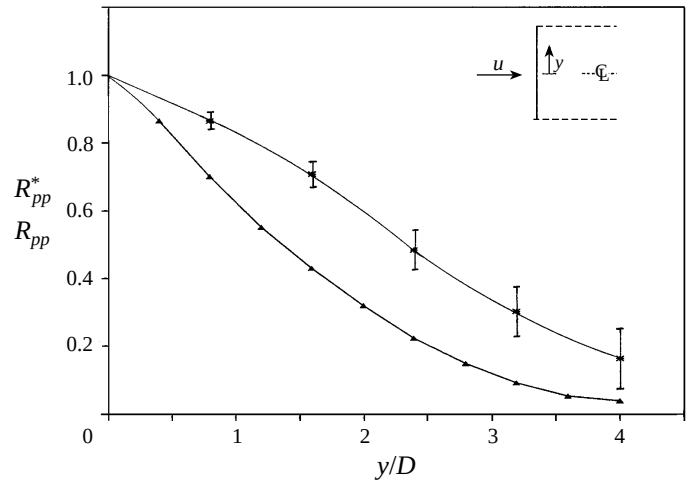

FIGURE 23. Cross-correlation of fluctuating pressure for time-averaged (▲) and conditionally sampled (*) data as a function of lateral displacement. $\sigma_u/\bar{u} = 0.080$. $L_x/D = 2.1$, vertical bars indicate 95% confidence interval.

correlation show up as spikes on the $p_1' p_1'$ trace as shown in figure 22. For an arbitrary time period, the cross-correlation coefficient can be calculated using the following expression:

$$R_{pp} = \frac{A_{12}}{(A_{11} A_{22})^{1/2}}, \tag{8}$$

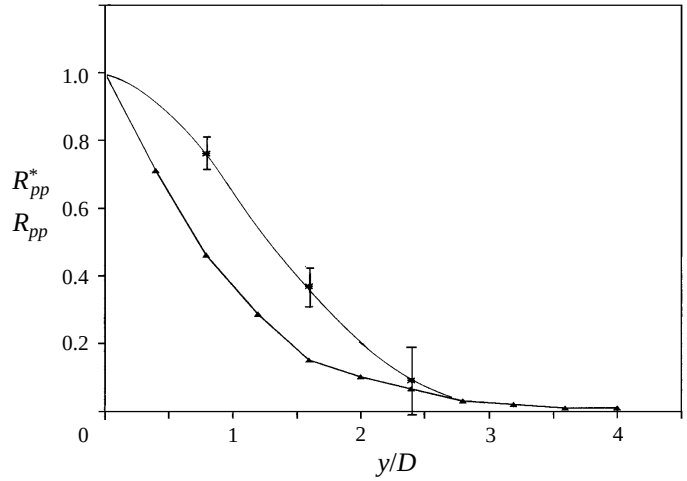

FIGURE 24. Cross-correlation of fluctuating pressure for time-averaged (▲) and conditionally sampled (*) data as a function of lateral displacement. $\sigma_u/\bar{u} = 0.082$, $L_x/D = 0.4$, vertical bars indicate 95% confidence interval.

where A_{12} is the area under the time trace $p'_1 p'_2$, A_{11} is the area under $p'_1 p'_1$, and A_{22} is the area under $p'_2 p'_2$. Equation (8) can be easily derived from the definition of the time-averaged cross-correlation coefficient, equation (7). Based on (8), a conditionally sampled cross-correlation coefficient, R^*_{pp}, was measured to obtain a quantitative estimate of the spanwise length of the largest vortices. For a sample of N negative peaks measured at tapping 1, the conditionally sampled correlation coefficient between pressure signals at tapping 1 and tapping 2 is:

$$R^*_{pp} = \frac{\sum_{i=1}^{N} (A_{12})_i}{\left[\sum_{i=1}^{N} (A_{11})_i * \sum_{i=1}^{N} (A_{22})_i\right]^{1/2}}. \tag{9}$$

A peak was arbitrarily defined as the segment between zero-crossings of positive and negative slope when the level $(\bar{p} - 4\sigma_p)$ was exceeded. The conditioning signal, p'_1, was measured at $x \approx 0.25 X_R$ on the model centreline.

Values of R_{pp} and R^*_{pp} as a function of lateral displacement are shown in figures 23–25 for the flows of figures 19, 20 and 21, respectively. Vertical bars through the data indicate 95% confidence intervals. A sample size, N, of between 100 and 300 peaks was used to estimate R^*_{pp}. For small separations ($y/D < 1.0$), a large peak at tapping 1 almost always coincided with a peak at tapping 2. In this case, a relatively small sample size was required to estimate R^*_{pp}. On the other hand, for large separations ($y/D > 2.0$), the vortex that produced a large peak at tapping 1 only occasionally affected tapping 2. Thus, a larger value of N was required as separation increased.

A comparison of figure 23 and figure 24 shows that decreasing turbulence scale by a factor of five significantly reduces the instantaneous spanwise correlation. In the small-scale flow, $R_{pp} \approx R^*_{pp} \approx 0.1$ at $y/D = 2.4$. Thus, even the most intense vortices extend over a relatively small spanwise distance. In the large-scale flow, however, $R^*_{pp} \approx 0.5$ at $y/D = 2.4$. Even at very large separation ($y/D = 4.0$), R^*_{pp} exceeds R_{pp}, indicating that spanwise vortices become more two-dimensional as turbulence scale increases. It should be noted that the value of L_X/D of 2.1 for the large-scale flow is

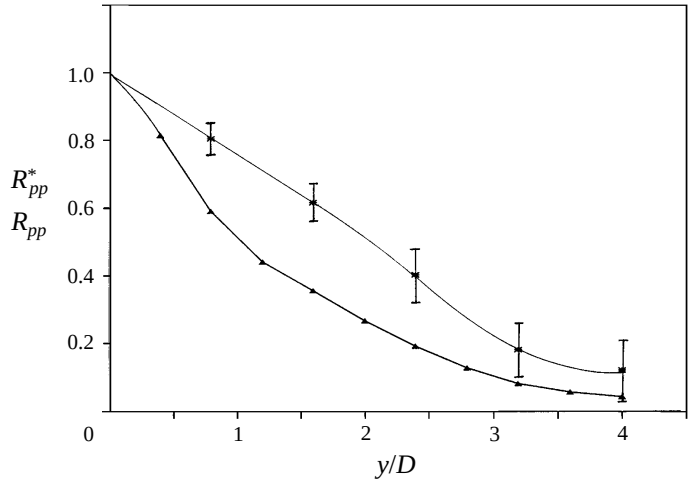

FIGURE 25. Cross-correlation of fluctuation pressure for time-averaged (▲) and conditionally sampled (*) data as a function of lateral displacement. (Undisturbed flow: $\sigma_u/\bar{u} = 0.008$, vertical bars indicate 95% confidence interval.)

relatively small compared to turbulence scales associated with the flow around buildings.

Values of R^*_{pp} obtained in the undisturbed flow, shown in figure 25, are generally slightly less than corresponding values obtained in the large-scale turbulent flow. Evidence of a spanwise instability in shear layers separating from leading edges has been noted by a number of researchers. Cherry *et al.* (1984) suggest that there is 'a weak tendency for out of phase shear layer "flapping" motions to develop over spanwise separations of $0.6X_R$.' Kiya & Sasaki (1985) also estimate that the lateral scale of vortices in the reattaching zone is approximately $0.6X_R$ (approximately $3.0D$ in the undisturbed flow).

The correlation length based on conditionally-sampled data, L^*_y, is approximately $2.4D$ in the large-scale flow and $1.4D$ in the small-scale flow. In the undisturbed flow, $L^*_y \approx 2.2D$. These values represent an increase of approximately 50% over correlation lengths obtained from time-averaged data, as shown in table 2. The increase in correlation length obtained from conditional sampling will, of course, depend on the threshold level chosen.

4. Conclusion

This experimental study has provided some information on the mechanism that produces large pressure fluctuations on streamwise surfaces of sharp-edged bluff bodies. Peak pressure fluctuations occur when free-stream perturbations cause the separated shear layer to roll up near the leading edge. At moderate Reynolds numbers ($Re > 10^4$), shear-layer roll-up occurs even in the undisturbed flow. An increase in $\sigma_u/\bar{u}$ produces stronger spanwise vortices and, as a result, increases the magnitude of pressure fluctuations.

An increase in turbulence scale increases the magnitude of pressure fluctuations in the separation bubble. This is a result of:

(i) An increase in spanwise coherence of vortices that are formed when the shear layer rolls up,

(ii) a decrease in perturbation frequency which increases the duration of vorticity entrainment.

A flow-visualization technique was developed which allowed detailed observation of the two-dimensional structure of the separation bubble. An advantage of this technique is that it allows the visualization of separated shear layers in highly turbulent flows. Although not presented in this paper, good results have been obtained in flows with $\sigma_u/\bar{u}$ exceeding 20 %. Although the mean wind velocity was only 12.3 m s^{-1} in the present study, the flow-visualization technique should be applicable at much higher flow speeds.

REFERENCES

Chandrsuda, C., Mehta, R. D., Weir, A. D. & Bradshaw, P. 1978 Effect of free-stream turbulence on large structure in turbulent mixing layers. *J. Fluid Mech.* **85**, 693–704.

Cherry, N. J. 1982 The effects of stream turbulence on a separated flow with reattachment. PhD thesis, Imperial College, University of London.

Cherry, N. J., Hillier, R. & Latour, M. E. M. P. 1984 Unsteady measurements in a separated and reattaching flow. *J. Fluid Mech.* **144**, 13–46.

Doligalski, T. L. & Walker, J. D. A. 1984 The boundary layer induced by a convected two-dimensional vortex. *J. Fluid Mech.* **139**, 1–28.

Gartshore, I. S. & Djilali, N. 1986 Flow separation – problems and possibilities. *9th Australasian Fluid Mech. Conf., Auckland, NZ.*

Gringorten, I. I. 1963 A plotting rule for extreme probability paper. *J. Geophys. Res.* **68**, 813–814.

Head, M. R. & Bandyopadhyay, P. 1981 New aspects of turbulent boundary layer structure. *J. Fluid Mech.* **107**, 297–338.

Hillier, R. & Cherry, N. J. 1981 The effect of stream turbulence on separation bubbles. *J. Wind Engng Ind. Aerodyn.* **8**, 49–58.

Hillier, R. & Dulai, B. S. 1985 Pressure fluctuations in a turbulent separated flow. *5th Symp. on Turbulent Shear Flows, Cornell University, Ithaca, NY.*

Holmes, J. D. 1984 Effect of frequency response on peak pressure measurements. *J. Wind Engng Ind. Aerodyn.* **17**, 1–9.

Hourigan, K., Thompson, M. C., Welsh, M. C. & Stokes, A. N. 1985 Discrete-vortex model of flow over a semi-infinite plate in a fluctuating field. *4th Intl Conf. on Numerical Methods in Laminar and Turbulent Flow, Swansea, UK.*

Hunt, A. 1982 Wind tunnel measurements of surface pressures on cubic building models at several scales. *J. Wind Engng Ind. Aerodyn.* **10**, 137–163.

Kiya, M. & Sasaki, K. 1983*a* Freestream turbulence effects on a separation bubble. *J. Wind Engng Ind. Aerodyn.* **14**, 375–386.

Kiya, M. & Sasaki, K. 1983*b* Structure of a turbulent separation bubble. *J. Fluid Mech.* **137**, 83–113.

Kiya, M. & Sasaki, K. 1985 Structure of large-scale vortices and unsteady reverse flow in the reattaching zone of a turbulent separation bubble. *J. Fluid Mech.* **154**, 463–491.

Lasheras, J. C., Cho, J. S. & Maxworthy, T. 1986 On the origin and evolution of streamwise vortical structures in a plane, free shear layer. *J. Fluid Mech.* **172**, 231–258.

Melbourne, W. H. 1979 Turbulence effects on maximum surface pressures – a mechanism and possibility of reduction. *Proc. 5th Intl Conf. on Wind Engng, Fort Collins, CO*, pp. 541–551.

Melbourne, W. H. 1982 Comparison of model and full scale tests of a bridge and a chimney stack. *Proc. Intl Workshop on Wind Tunnel Modeling, Gaithersburg, MD*, pp. 637–653.

Merzkirch, W. 1974 *Flow Visualization*. Academic Press, New York, NY.

Milne-Thompson, L. M. 1960 *Theoretical Hydrodynamics*, 4th edn, Macmillan.

Nakamura, Y. & Ozono, S. 1987 The effects of turbulence on a separated and reattaching flow. *J. Fluid Mech.* **178**, 477–490.

Parker, R. & Welsh, M. C. 1983 Effects of sound on flow separation from blunt flat plates. *Intl J. Heat and Fluid Flow* **4**, 113–127.

Saathoff, P. J. & Melbourne, W. 1987 Freestream turbulence and wind tunnel blockage effects on streamwise surface pressures. *J. Wind Engng Ind. Aerodyn.* **26**, 353–370.

Saathoff, P. J. 1989 Effects of free-stream turbulence on surface pressure fluctuations in separated/reattaching flows. PhD thesis, Monash University.

Sigurdson, L. W. & Roshko, A. 1985 Controlled unsteady excitation of a reattaching flow. *AIAA Shear Flow Control Conf.*, *Boulder*, *CO*.